THE JOURNAL OF PHYSICAL CHEMISTRY B

Article

Cite This: J. Phys. Chem. B 2018, 122, 7416−7425

pubs.acs.org/JPCB

Network Structure and Connectivity in $SnO-P_2O_5$ Glasses: Results from 2D ^{31}P and ^{119}Sn NMR Spectroscopy

Yiqing Xia,[†] Maxwell A. T. Marple,[†] Ivan Hung,[‡] Zhehong Gan,[‡] and Sabyasachi Sen*[,†]

[†]Department of Materials Science & Engineering, University of California at Davis, Davis, California 95616, United States

[‡]Center of Interdisciplinary Magnetic Resonance, National High Magnetic Field Laboratory, 1800 East Paul Dirac Drive, Tallahassee, Florida 32310, United States

ABSTRACT: The compositional evolution of the network structure and connectivity in binary $SnO-P_2O_5$ glasses with $35 \leq$ mol % $SnO \leq 55$ is studied using two-dimensional ^{119}Sn and ^{31}P NMR spectroscopy. The phosphate Q^n species concentrations, as obtained from the analyses of the ^{31}P NMR spectral line shapes suggest that the network modification can be described in terms of a binary Q-speciation model. On the other hand, the ^{119}Sn NMR spectra suggest that the Sn−O coordination environment in these glasses is composition dependent. Sn is present in both 3-fold (trigonal pyramid) and 4-fold (trigonal bipyramid) coordinations with oxygen in these glasses. The relative fraction of the trigonal pyramidal environment increases with increasing SnO content. The unusually low glass transition temperature T_g of these glasses (241−266 °C) is argued to be related to the low coordination number of Sn, leading to a relatively sparsely connected structural network.

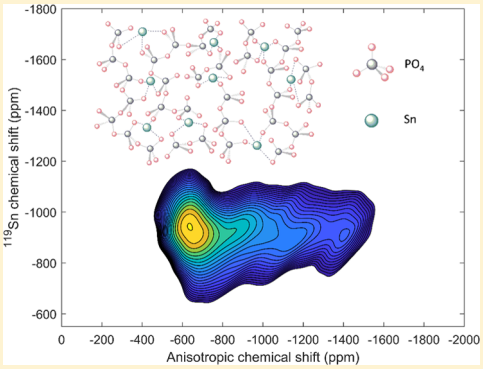

1. INTRODUCTION

Phosphate glasses are characterized by several unique properties including low processing temperature, large solubility of rare earth and other high-field-strength cations, and large thermal expansion coefficient, making them candidates for a variety of technological applications, including solid state electrolytes, nuclear waste encapsulation, glass-to-metal sealing, and solid-state laser host materials.[1−4] Interest in tin phosphate ($SnO-P_2O_5$) glasses is driven primarily by their high refractive index, zero stress-optic response, and low glass transition temperature T_g, making them suitable for applications in optics as well as in low-temperature glass-to-metal sealing.[5−9] The structure of tin phosphate glasses has been investigated extensively in recent years using a variety of characterization techniques including infrared and Raman spectroscopy as well as ^{31}P and ^{119}Sn NMR spectroscopy.[9]

^{31}P magic-angle-spinning (MAS) NMR spectroscopic measurements played a key role in the identification and quantitation of the various PO_4 Q^n species in phosphate glasses, where n represents the number of bridging oxygen (BO) atoms in each PO_4 tetrahedron. However, unlike alkali, alkaline-earth, Zn-, or Pb-phosphate glasses, the ^{31}P MAS NMR spectra of the tin phosphate glasses display strongly overlapping resonances corresponding to various Q species, making an unequivocal quantitation of the latter via simulation of the spectral line shapes a challenging task. Additional structural information including the phosphorus site symmetry and conformation for the PO_4 tetrahedra in various Q^n species can only be gained from the determination of the full ^{31}P chemical shift tensor.[10] On the other hand, ^{119}Sn NMR spectroscopy was also used in previous studies to obtain the local environment of Sn in tin phosphate glasses.[7,11] However, the static ^{119}Sn NMR spectra reported in these studies were simultaneously broadened by chemical shift dispersion and anisotropy, and deconvolution of these two effects is impossible in one-dimensional NMR spectra. In contrast, the two-dimensional (2D) isotropic−anisotropic correlation NMR experiments, such as magic-angle turning (MAT)[12] and phase-adjusted spinning sidebands (PASS),[13] can separate the isotropic and anisotropic chemical shift information in two dimensions and allow for the determination of their correlation in a single experiment. Here, we report the results of 2D ^{31}P and ^{119}Sn isotropic−anisotropic correlation NMR spectroscopic studies of the structure of $(SnO)_x(P_2O_5)_{100-x}$ glasses with $35 \leq x \leq 55$. These results are analyzed to build a model of the compositional evolution of the structure of these glasses. The variation in the molar volume and T_g of these glasses with composition is shown to be consistent with the proposed structural model.

2. EXPERIMENTAL METHODS

2.1. Sample Preparation and Physical Characterization. The $(SnO)_x(P_2O_5)_{100-x}$ glasses with $35 \leq x \leq 55$ were prepared in 10 g batches from $Sn_2P_2O_7$ (Alfa) and P_2O_5 (J. T. Baker). In previously published literature,[7] significant amounts of Sn^{4+} and water were detected in the tin phosphate

Received: May 3, 2018
Revised: June 26, 2018
Published: June 27, 2018

DOI: 10.1021/acs.jpcb.8b04236
J. Phys. Chem. B 2018, 122, 7416−7425

glasses. In the present study, we have exercised caution in avoiding air and moisture during the synthesis of the $SnO-P_2O_5$ glasses. The $Sn_2P_2O_7$ reagent was heated in a silica ampoule and held at 200 °C for 1 h under vacuum to remove any water. $Sn_2P_2O_7$ was subsequently transferred to a nitrogen-purged glovebox, where it was mixed with stoichiometric quantity of P_2O_5. These batches were taken in an evacuated fused silica ampoule and melted in a rocking furnace at 1000 °C for 30 min. These melts were then quenched by dipping the ampoule in water. Resulting glass samples were stored in the glovebox to avoid any exposure to atmospheric moisture as tin phosphate glasses are quite hygroscopic in nature. All subsequent handling of these glasses for various experiments was also carried out inside the glovebox. The chemical composition of the resulting glasses was determined via electron probe microanalysis (Cameca SX-100) and the SnO and P_2O_5 concentrations were found to be within ±0.2 mol % of their nominal values. Therefore, the nominal compositions of these glasses are used in the subsequent discussion. Furthermore, no Si was detected in these chemical analyses, suggesting a negligible reaction between the melt and SiO_2 ampoule during the relatively short melting time used in this study. The T_g of these tin phosphate glasses was measured using a Mettler Toledo DSC1 differential scanning calorimeter. These measurements were carried out in a flowing nitrogen environment on 15−25 mg samples that were taken in Al pans and heated at a rate of 10 K/min; T_g was taken as the onset of the glass transition endotherm. Density of these glasses with a low tin content ($x < 50$) was measured using the Archimedes' method with toluene as the immersion medium and that of the glasses with a high tin content ($x \geq 50$) was measured using a pycnometer (Micromeritics AccuPyc II 1340) with helium as the displacement gas. All the density measurements were carried out at 20 °C. All the reported densities are averages of 10 consecutive measurements on each sample.

2.2. ^{31}P NMR Measurements. The ^{31}P MAS NMR spectra of all the glasses were collected using a Bruker DRX spectrometer, equipped with a 31 mm bore magnet operating at 19.6 T (^{31}P Larmor frequency of 336.6 MHz), at the National High Magnetic Field Laboratory (NHMFL). Crushed glass samples were spun at 15 kHz in ZrO_2 rotors with a 3.2 mm HX MAS probe designed and built at the NHMFL. Each ^{31}P MAS spectrum is the Fourier transform of 32 free induction decays acquired with a Hahn-echo pulse sequence using $\pi/2$- and π-pulses of 2.5 and 5 μs, respectively, and a recycle delay of 300 s. All the ^{31}P PASS NMR measurements were performed using a Bruker Avance500 spectrometer and a Bruker magnet operating at 11.7 T (^{31}P Larmor frequency of 202.44 MHz). The crushed glass samples were taken in 4 mm ZrO_2 rotors and spun at 6 kHz using a Bruker triple-resonance MAS probe. The 2D PASS pulse sequence consists of a $\pi/2$ pulse (2.15 μs) followed by a train of π pulses with the rotor-synchronized interpulse delays following the solutions of the PASS equations.[13] A 12-step cogwheel phase cycle was used to eliminate the effects of pulse imperfections.[14] Each 2D PASS spectrum was obtained using 16 t_1 points with 12 transients per point, and a recycle delay of 600 s. All the ^{31}P spectra were externally referenced to 85% H_3PO_4 with δ_{iso} at 0 ppm. The spectral line shapes of ^{31}P MAS and PASS NMR experiments were analyzed using the software DMFit.[15]

2.3. ^{119}Sn NMR Measurements. ^{119}Sn NMR spectra are typically characterized by large chemical shift anisotropy (CSA) and chemical shift range. In the present study, we employ the ^{119}Sn projection magic-angle turning/Carr−Purcell−Meiboom−Gill (pjMAT/CPMG) NMR spectroscopy to separate the CSA from the isotropic chemical shift to study the coordination environment of Sn in the tin phosphate glasses. The pjMAT/CPMG NMR experiment provides identical information as the PASS NMR described above,[16,17] but uses magic-angle turning and projection pulses to sample a large chemical shift range, making it an ideal sequence for ^{119}Sn NMR in glasses. Additionally, the application of Carr−Purcell−Meiboom−Gill (CPMG) echo train acquisition of the pjMAT data drastically reduces the experimental time such that a high-resolution spectrum for low natural abundance nuclides, such as ^{119}Sn (8.6%), can be acquired within a reasonable time span.[18,19] The specific pulse sequence timings are detailed elsewhere.[18] All the ^{119}Sn NMR measurements were carried out at the NHMFL, on a 31 mm bore magnet equipped with a Bruker DRX console, operating at 19.6 T (^{119}Sn Larmor frequency of 309.8 MHz) and a 3.2 mm HX MAS probe designed and built at the NHMFL. The crushed glass samples were spun at 10 kHz in ZrO_2 rotor. Each ^{119}Sn 2D pjMAT/CPMG spectrum was obtained using an indirect dimension spectral window of 320 kHz, 10 hypercomplex t_1 data points with 648 transients per point, 83 CPMG echoes per transient, and a recycle delay of 25 s. A 2.5 μs duration was used for all the pulses in the pulse sequence. All the spectra were referenced to $SnMe_4$ with δ_{iso} at 0 ppm by recording the ^{17}O signal of neat, natural abundance H_2O and then using the frequency ratios reported in the IUPAC recommendations.[20] The projections along the isotropic and anisotropic dimensions were simulated using the software DMFit.[15]

The ^{31}P and ^{119}Sn CSA tensors reported here are defined using the Haeberlen convention[21] as

$$|\delta_{zz} - \delta_{iso}| \geq |\delta_{xx} - \delta_{iso}| \geq |\delta_{yy} - \delta_{iso}|$$

$$\delta_{iso} = \frac{1}{3}(\delta_{zz} + \delta_{xx} + \delta_{yy})$$

$$\delta = \delta_{zz} - \delta_{iso}$$

$$\eta = \frac{\delta_{yy} - \delta_{xx}}{\delta}$$

where δ_{xx}, δ_{yy}, and δ_{zz} are the principle components of the CSA tensor and δ_{iso} is the isotropic chemical shift. The magnitude of the anisotropy is δ, whereas its asymmetry is denoted by η.

3. RESULTS AND DISCUSSION

3.1. Physical Properties. The T_g of $SnO-P_2O_5$ glasses measured in this study are in good agreement with those reported in the literature (Figure 1).[7,22] Although, when taken together, the T_g of these glasses appears to increase slightly with increasing SnO content, no significant trend is observed in the composition range investigated in the present study (Figure 1). As noted by Lim et al.,[9] the T_g of $SnO-P_2O_5$ glasses are 100−200 °C lower than that of other low-T_g binary phosphate glasses of similar stoichiometry, in the systems $ZnO-P_2O_5$ and $PbO-P_2O_5$.[7] The compositional dependence of the molar volume of the $SnO-P_2O_5$ glasses is shown in Figure 2. The results are in good agreement with those reported in previous studies; the molar volume decreases in a near-linear fashion, with increasing amount of SnO, suggesting an increase in the atomic packing with increasing network modification.[11]

DOI: 10.1021/acs.jpcb.8b04236
J. Phys. Chem. B 2018, 122, 7416−7425

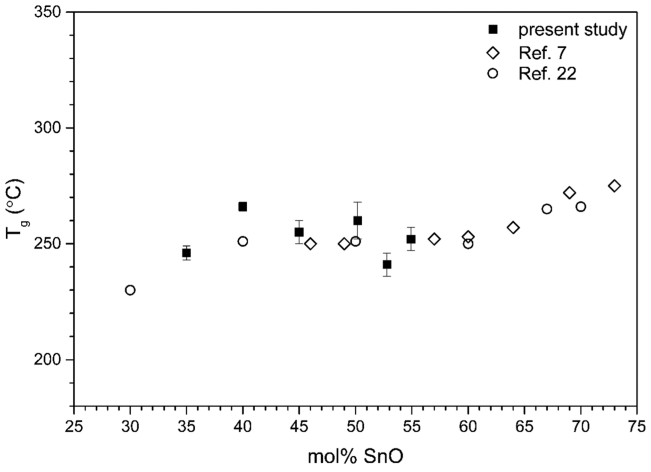

Figure 1. Glass transition temperature of $SnO-P_2O_5$ glasses measured in the present study (squares) and reported in the literature (circles and diamonds).

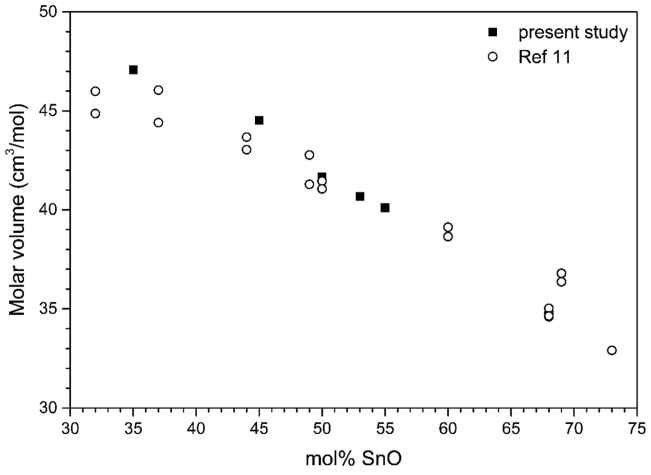

Figure 2. Molar volume of $SnO-P_2O_5$ glasses measured in the present study (squares) and reported in the literature (circles). Experimental uncertainties are within the size of the symbols.

3.2. ^{31}P NMR. The ^{31}P MAS NMR spectra of the $SnO-P_2O_5$ glasses are shown in Figure 3a. It is clear that both isotropic line shape (center band) and sideband pattern and intensity distribution change progressively with composition, indicating a corresponding evolution of the Q^n speciation. The compositional evolution of the center band is shown in detail in Figure 3b, which displays an increase in relative intensity on the high parts per million side with increasing SnO content, corresponding to a progressive replacement of the Q^3 species with Q^2 and Q^1 species (see below). Each of these center bands can be simulated well with a minimum of two Gaussian components corresponding to two distinct Q^n species. However, such simulations are rather nonunique and require one to arbitrarily constrain the peak positions and/or width to obtain self-consistent results. Therefore, ^{31}P 2D PASS experiments were carried out to obtain a more accurate compositional evolution of the Q^n speciation.

The representative ^{31}P 2D PASS NMR spectra of these $SnO-P_2O_5$ glasses are shown in Figure 4. It may be noted that the projection of these spectra along the isotropic dimension is free of any CSA-induced broadening. On the other hand, the CSA information for any isotropic shift can be obtained from

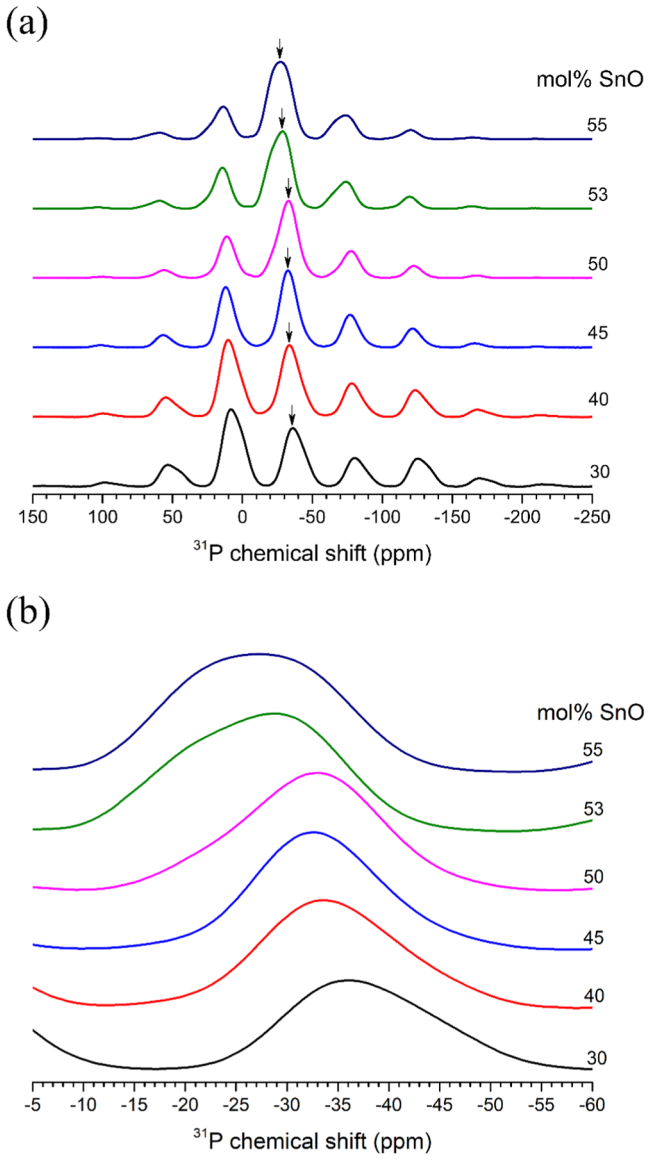

Figure 3. (a) High-field (19.6 T) ^{31}P MAS NMR spectra of $SnO-P_2O_5$ glasses. The isotropic peak in each spectrum is indicated by arrow, whereas all the other peaks are spinning sidebands. (b) Expanded view of the isotropic peaks in (a). Glass compositions are indicated alongside the spectra.

the slices of these spectra along the anisotropic dimension. A strong overlap of the peaks corresponding to different Q^n species is also evident in the isotropic spectra of these glasses (Figure 4). Previous ^{31}P NMR studies of phosphate glasses have shown that the various Q species differ significantly in their characteristic δ and η values.[23,24] Therefore, the variation in the chemical shift tensor parameters δ and η with δ_{iso} is analyzed for each glass composition to constrain the Q^n isotropic peak positions because the latter should closely correspond to the δ_{iso} values corresponding to the extrema in δ and η. Examples of such analyses are shown in Figure 5, where the sideband spikelet patterns for slices along the anisotropic dimension in the ^{31}P 2D PASS NMR spectrum of the $53SnO-47P_2O_5$ glass are simulated to extract the parameters δ and η.[15] The correlations between δ and δ_{iso} and those between η and δ_{iso} of typical ultraphosphate glasses ($35SnO-65P_2O_5$) and polyphosphate glasses ($53SnO-47P_2O_5$) are shown in Figure

DOI: 10.1021/acs.jpcb.8b04236
J. Phys. Chem. B 2018, 122, 7416−7425

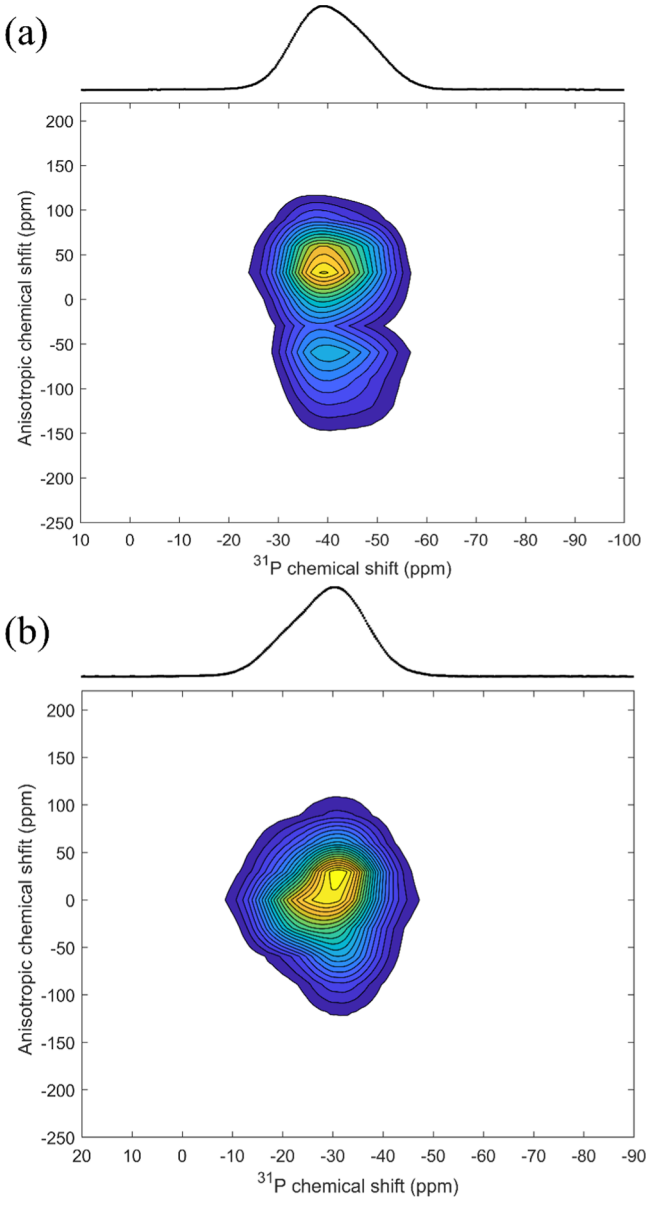

Figure 4. Contour plot of representative ^{31}P 2D PASS NMR spectra of (a) $35SnO-65P_2O_5$ and (b) $53SnO-47P_2O_5$ glasses. Projections along the isotropic (horizontal) dimension are shown on the top.

6. It is clear from Figure 6a that for the ultraphosphate glass, δ and η display a non-monotonic variation with clear extrema near −47 and −35 ppm, which correspond well with the average δ_{iso} of the Q^3 and the Q^2 species, respectively. On the other hand, in the case of the polyphosphate glass, the minimum in η near −18 ppm corresponds to the average δ_{iso} of the Q^1 species. It may be noted here that in Figure 6b, the sharp peak in η near −25 ppm is an artifact of the CSA tensor convention used in this study, as this peak location corresponds to δ_{iso}, where δ switches its sign, corresponding to the appearance of the signal from the Q^1 species. These average δ_{iso} and the corresponding δ and η values are used to simulate the ^{31}P one-pulse MAS spectra of all $SnO-P_2O_5$ glasses in a self-consistent fashion (Figure 7). These simulation parameters are listed in Table 1. The Q speciation thus obtained is shown in Figure 8, which clearly follows a binary model of progressive modification of a Q^3 phosphate network, with increasing addition of the modifier SnO.[25]

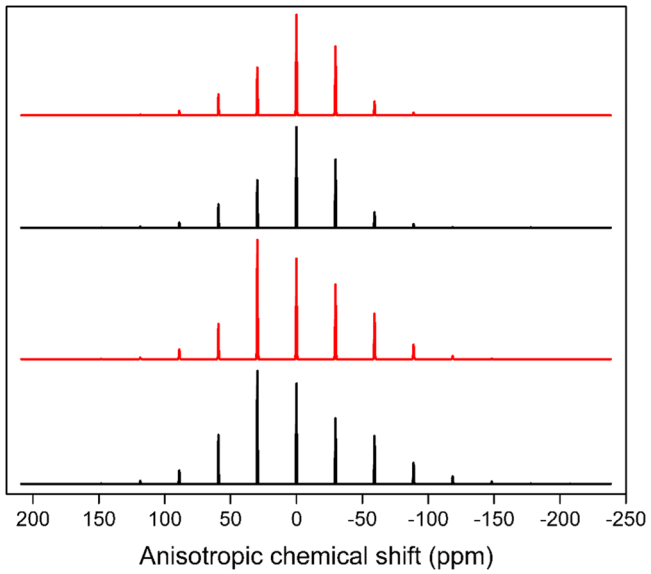

Figure 5. Experimental (black) and simulated (red) anisotropic ^{31}P NMR sideband spikelet patterns of $53SnO-47P_2O_5$ glass, taken at δ_{iso} = −18.55 ppm (top) and δ_{iso} = −32.72 ppm (bottom).

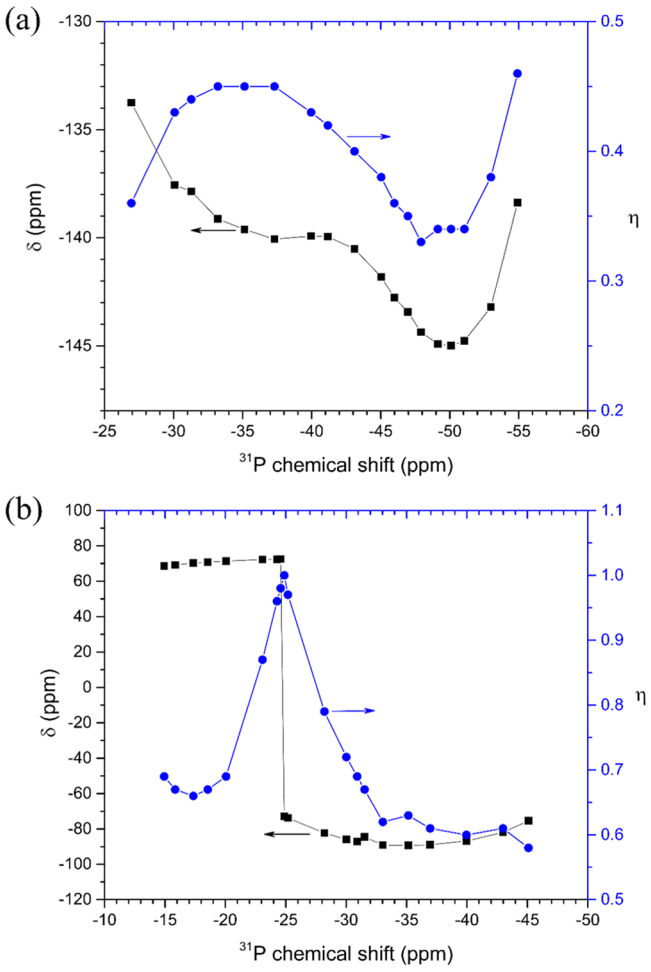

Figure 6. Variation in δ (black square) and η (blue circle) with δ_{iso} for (a) $35SnO-65P_2O_5$ and (b) $53SnO-47P_2O_5$ glasses. Lines through the data points are guides to the eye.

It is interesting to note here that the Q^2 species, which is the most dominant Q species in all the glasses in the composition

DOI: 10.1021/acs.jpcb.8b04236
J. Phys. Chem. B 2018, 122, 7416−7425

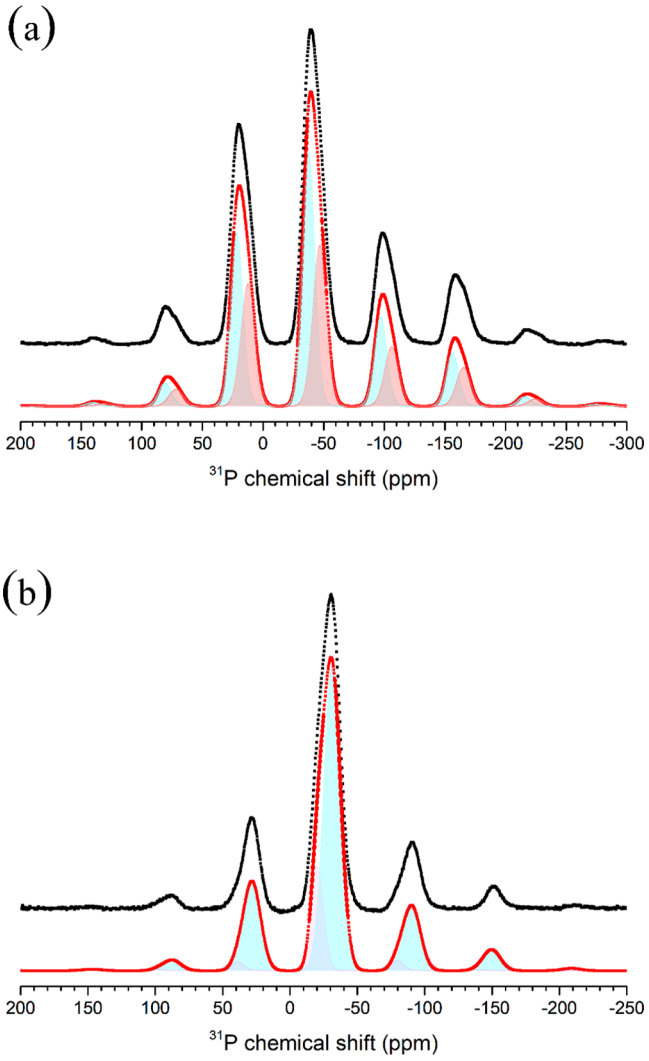

Figure 7. Representative simulations of ^{31}P MAS NMR spectral line shapes of (a) $35SnO-65P_2O_5$ and (b) $53SnO-47P_2O_5$ glasses. Experimental (black) and simulated (red) line shapes are shown along with the Gaussian simulation components corresponding to various Q species: Q^1 (light blue); Q^2 (teal); and Q^3 (light pink).

range explored in the present study, displays interesting changes in its NMR parameters with composition (Figure 9). First of all, the full width at half-maximum (FWHM) of the Q^2-peak in the ^{31}P NMR spectra abruptly increases from

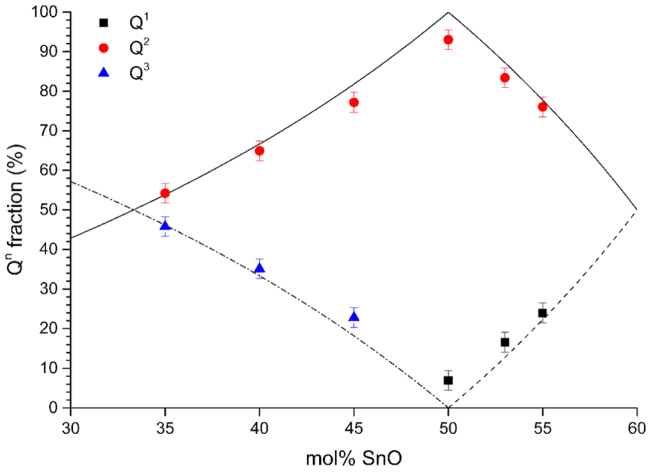

Figure 8. Q^n speciation in $SnO-P_2O_5$ glasses determined from ^{31}P NMR data. Dot-dashed, solid, and dashed lines are relative fractions of Q^3, Q^2, and Q^1, respectively, expected from a binary model.

ultraphosphate to polyphosphate glasses as the SnO content becomes ≥50 mol % (Figure 9a). This result is possibly indicative of a greater conformational disorder of phosphate chains in polyphosphate glasses where the chains have higher degrees of configurational freedom. On the other hand, the $|\delta|$ value for the Q^2 species decreases, whereas η increases nearly linearly with increasing SnO content (Figure 9b,c). The parameters $|\delta|$ and η increase with increasing departure of the chemical shift tensor from spherical and uniaxial symmetry, respectively. Therefore, the observed trends of $|\delta|$ and η in $SnO-P_2O_5$ glasses suggest that the ^{31}P chemical shift tensor for the Q^2 species becomes more spherically symmetric and nonaxial with increasing SnO content. As such, the Q^2 phosphorus site is expected to have a nonaxial symmetry with relatively large $|\delta|$ and η, as the P atom is coordinated to two nonbridging oxygen (NBO) and two bridging oxygen (BO) and forms a double bond with one of the NBO atom. Because this basic conformation of the Q^2 PO_4 tetrahedron remains unchanged in all the glasses irrespective of their composition, the monotonic relative variation in $|\delta|$ and η with SnO content in Figure 9b,c may reflect a complex effect of Sn modifier cations on the P−O bond lengths and P−O−P bond angles in the Q^2 chains. Further experimental and computational studies are needed for a complete understanding of these effects.

Table 1. ^{31}P MAS NMR Line Shape Simulation Parameters for $SnO-P_2O_5$ Glasses

glass composition	Q^n species	δ_{iso} (ppm)	FWHM (±0.5 ppm)	Q^n fraction (±1%)	δ (ppm) ±10%	η (±0.05)
$35SnO-65P_2O_5$	Q^3	−43.3	14.3	46	−146.0	0.10
	Q^2	−33.7	12.6	54	−133.5	0.32
	Q^3	−41.3	14.3	35	−140.0	0.23
	Q^2	−32.4	13.0	65	−124.0	0.36
	Q^3	−39.3	14.5	23	−124.0	0.35
	Q^2	−31.5	12.9	77	−111.0	0.46
	Q^2	−33.3	14.8	93	−97.8	0.55
	Q^1	−21.3	11.0	7	55.0	0.60
	Q^2	−29.7	14.8	83	−98.0	0.56
	Q^1	−18.8	11.0	17	62.0	0.62
	Q^2	−30.3	15.0	76	−90.9	0.63
	Q^1	−20.2	11.0	24	63.0	0.80

DOI: 10.1021/acs.jpcb.8b04236
J. Phys. Chem. B 2018, 122, 7416−7425

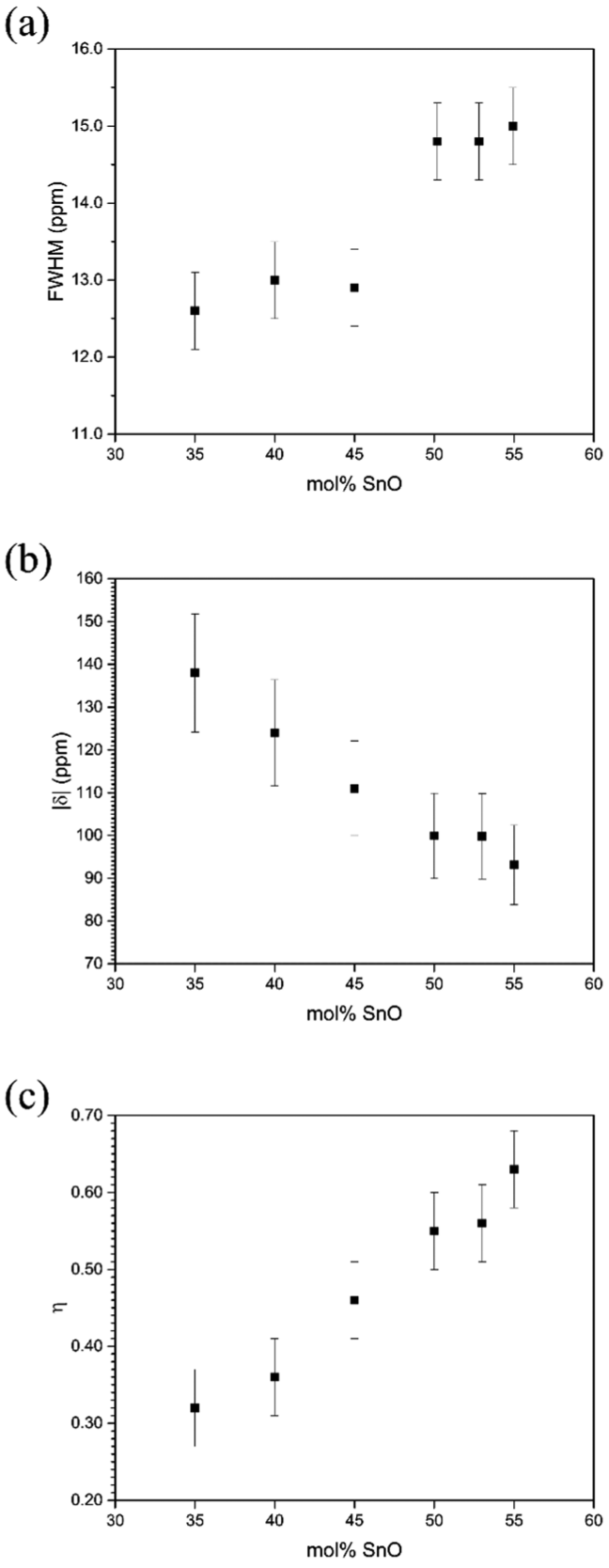

Figure 9. Compositional variation in (a) FWHM (b) average $|\delta|$ and (c) average η of Q^2 resonance in $SnO-P_2O_5$ glasses.

3.3. ^{119}Sn NMR. The contour plots of typical 2D ^{119}Sn pjMAT/CPMG NMR spectra of these $SnO-P_2O_5$ glasses and the corresponding isotropic projections are shown in Figures 10 and 11. We note at the outset that none of these spectra show any detectable amount of Sn to be present as Sn^{4+} in these glasses in environments similar to that in crystalline SnO_2 ($\delta_{iso} \approx -600$ ppm) or SnP_2O_7 ($\delta_{iso} \approx -770$ ppm), which

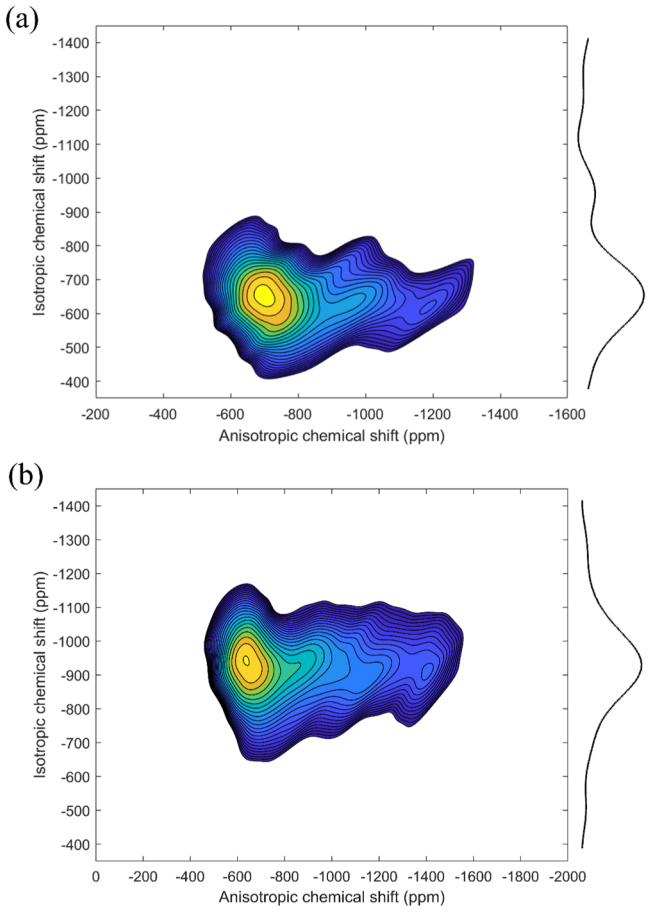

Figure 10. Contour plot of representative ^{119}Sn 2D pjMAT/CPMG NMR spectra of (a) $35SnO-65P_2O_5$ and (b) $53SnO-47P_2O_5$ glasses. Total projection along the isotropic (vertical) dimension is shown on the right side of each spectrum.

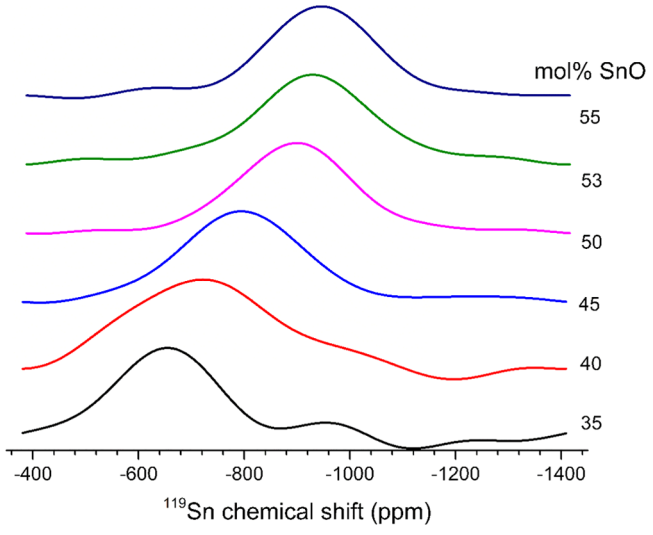

Figure 11. Isotropic projections of ^{119}Sn 2D pjMAT/CPMG NMR spectra of $SnO-P_2O_5$ glasses. Glass composition in terms of mol % SnO is denoted alongside the spectra.

DOI: 10.1021/acs.jpcb.8b04236
J. Phys. Chem. B 2018, 122, 7416−7425

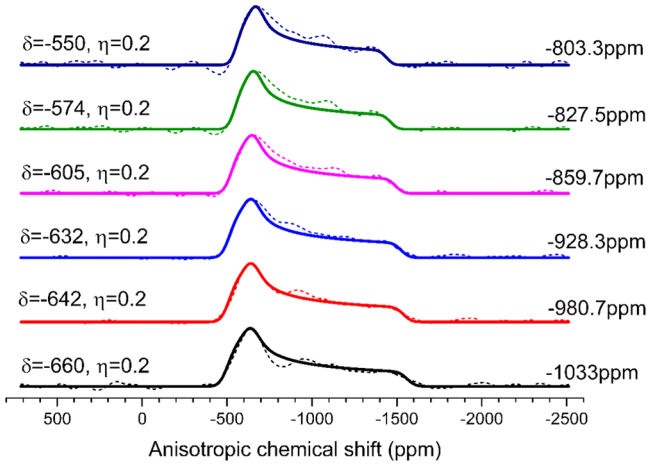

Figure 12. Experimental (dashed line) and simulated (solid lines) anisotropic ^{119}Sn NMR spectral line shapes of $53SnO-47P_2O_5$ glass taken from the ^{119}Sn 2D pjMAT/CPMG NMR spectrum at different δ_{iso} values indicated on the right, alongside each line shape. The simulated δ (parts per million) and η of ^{119}Sn chemical shift tensor are shown on the left.

Table 2. ^{119}Sn NMR Line Shape Simulation Parameters for $SnO-P_2O_5$ Glasses and Related Crystalline Compounds

glass/crystalline compounds	average δ_{iso} (ppm)	δ (ppm)[a] ±10%	η (±0.05)[a]
$35SnO-65P_2O_5$	−655	−470	0.38
$40SnO-60P_2O_5$	−719	−512	0.31
$45SnO-55P_2O_5$	−796	−567	0.25
$50SnO-50P_2O_5$	−900	−601	0.24
$53SnO-47P_2O_5$	−928	−632	0.22
$55SnO-45P_2O_5$	−944	−655	0.19
$Sn_2P_2O_7$[7]	−865		
$Sn_3(PO_4)_2$[7]	−624		
SnO[26]	−208	−656	0.00

[a]δ and η are obtained from the slices taken at δ_{iso} at the peak maximum.

would have resulted in relatively sharp resonances near the corresponding δ_{iso} values.[11,26] This result is consistent with the preparation of these glasses under anaerobic environment. The slices along the anisotropic dimension of the 2D spectrum of each composition were simulated at various δ_{iso} values (Figure 12) to obtain the parameters δ and η. Typical variations in δ and η with δ_{iso} are shown in Figure 12, and the δ and η values taken at the isotropic peak maximum for all compositions are listed in Table 2. The ^{119}Sn δ_{iso} at the isotropic peak maximum for these glasses become increasingly negative (−655 to −944 ppm) with increasing SnO content. However, they all fall in the range characteristic of Sn^{2+} in a trigonal pyramidal environment, as exemplified by the structures of crystalline β-$Sn_2P_2O_7$ and $Sn_3(PO_4)_2$ (Table 2).[26,27] As can be seen in Table 2, the ^{119}Sn δ_{iso} values for these trigonal pyramidal Sn environments are quite different from the (−208 ppm) characteristic of the 4-fold coordinated Sn atoms in a highly symmetric environment with Sn−O−Sn linkages, in the litharge structure of crystalline SnO.[26,28] This difference is expected because the electronic structure of Sn in SnO is expected to be rather different from that in Sn phosphates.[5] In this regard, a more relevant structure with a 4-fold coordinated Sn would be that of crystalline $K_2SnP_2O_7$, where Sn^{2+} ions exist in a trigonal bipyramidal environment, with a pair of short (2.12−2.14 Å) and a pair of long (2.35−2.39 Å) Sn−O distances.[29,30] Unfortunately, no ^{119}Sn NMR data are available in the literature for such Sn environments in this or any other Sn-phosphate compounds. To address this issue, we have performed ab initio calculations, based on the density functional theory, of the ^{119}Sn chemical shift tensor parameters for the 3-fold and 4-fold coordinated Sn sites in the crystal structures of β-$Sn_2P_2O_7$, $Sn_3(PO_4)_2$, and $K_2SnP_2O_7$,[27,29,31] without further geometry optimization. These tensor parameters are calculated using the gauge-including projector augmented wave method[32] within the generalized gradient approximation, as implemented in the code CASTEP-NMR (Biovia Inc.). An energy cutoff of 600 eV was used and the Brillouin zone was sampled using the Monkhorst−Pack scheme and a 4 × 4 × 4 k-point grid. These calculations yield the principal components σ_{xx}, σ_{yy}, and σ_{zz} of the absolute shielding tensor. The ^{119}Sn δ_{iso} was obtained from the isotropic shielding σ_{iso} using the relationship: $\delta_{iso} = -(\sigma_{iso} - \sigma_{ref})$, where σ_{ref} is the isotropic shielding of a reference material. The litharge structure of SnO was used as a reference and the calculated ^{119}Sn σ_{iso} of the single Sn site in this allotrope (3106 ppm) is equated to the experimental δ_{iso} value of −208 ppm.[26,28]

The results of these calculations are listed in Table 3. Clearly, the ^{119}Sn δ_{iso} or $|\delta|$ does not show any obvious trend with the Sn−O coordination number or bond distance. It may be noted here that the Sn atoms in some of the trigonal pyramidal environments in the crystal structures of β-$Sn_2P_2O_7$ and $Sn_3(PO_4)_2$ also have one or two distant oxygen neighbors at ∼3.0 Å, besides their three nearest oxygen neighbors at distances ranging between 2.1 and 2.3 Å. Whether these distant Sn−O pairs have bonded interactions or not remains an open question, but their effect on the ^{119}Sn chemical shift parameters

Table 3. Calculated ^{119}Sn NMR Chemical Shift Tensor Parameters for Crystalline Compounds

crystalline compounds	Sn coordination environment	Sn site	Sn−O distances (Å)	δ_{iso} (ppm)	$\lvert\delta\rvert$ (ppm)	η
$K_2SnP_2O_7$[29]	trigonal bipyramidal	Sn(1)	2.14, 2.12, 2.35, 2.39	−623	409	0.26
$Sn_2P_2O_7$[24]	trigonal pyramidal	Sn(1)	2.11, 2.23, 2.19, (2.86)[a]	−832	372	0.14
		Sn(2)	2.13, 2.14, 2.23	−690	443	0.07
		Sn(3)	2.13, 2.13, 2.12	−660	441	0.11
		Sn(4)	2.14, 2.14, 2.15	−810	401	0.03
$Sn_3(PO_4)_2$[27]	trigonal pyramidal	Sn(1)	2.12, 2.12, 2.12 (2.96, 2.98)[a]	−626	498	0.17
		Sn(2)	2.10, 2.10, 2.12 (3.05)[a]	−535	525	0.17
		Sn(3)	2.15, 2.23, 2.32 (2.86, 2.86)[a]	−800	439	0.03
SnO[33]	trigonal bipyramidal	Sn(1)	4 × 2.21	−208	467	0.00

[a]Distant oxygen neighbors.

DOI: 10.1021/acs.jpcb.8b04236
J. Phys. Chem. B 2018, 122, 7416−7425

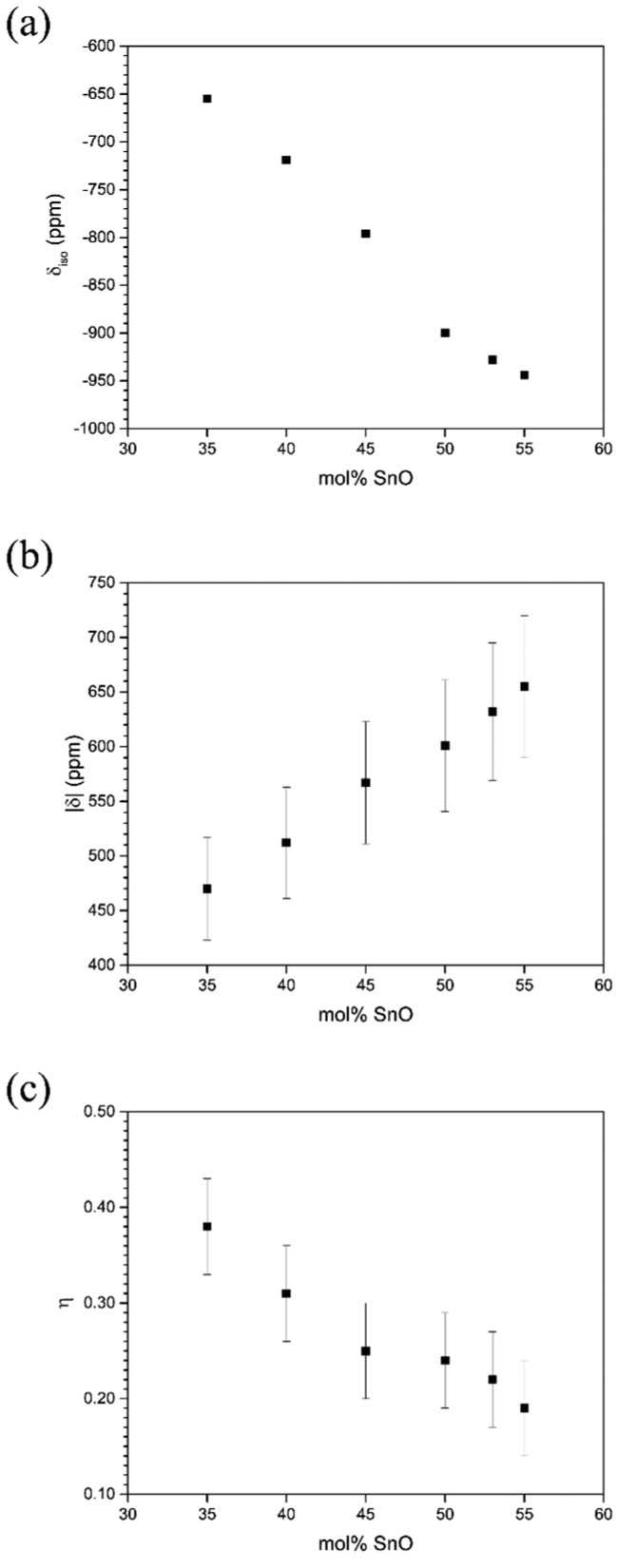

Figure 13. Compositional variation in average (a) δ_{iso}, (b) $|\delta|$, and (c) η of ^{119}Sn chemical shift tensor in $SnO-P_2O_5$ glasses.

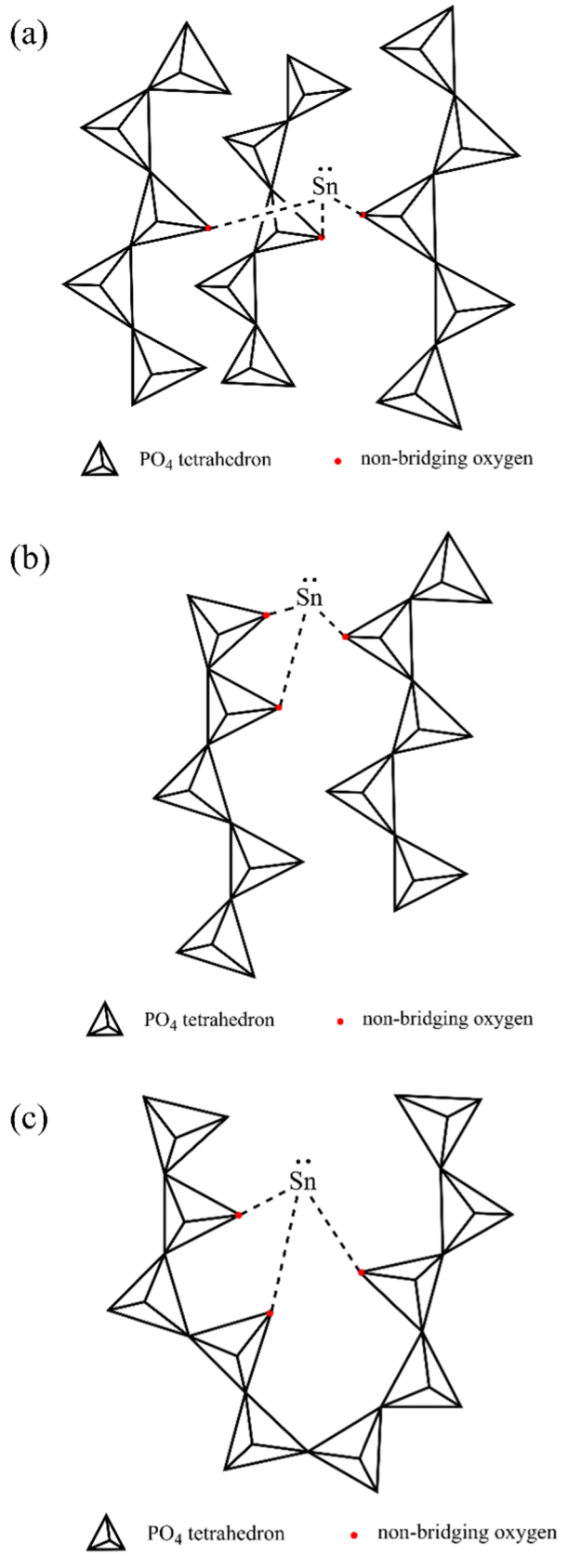

Figure 14. Cartoon representation of various possible cross-linking or connectivity schemes of Q^2 phosphate chains in glasses via Sn–$(NBO)_3$ trigonal pyramids: (a) maximal connectivity by cross-linking three chains; (b) moderate connectivity by cross-linking two chains; and (c) minimal connectivity when all three NBOs reside on the same puckered chain.

appear to be insignificant (Table 3). A closer inspection of the data in Table 3, however, indicates that the average δ_{iso} for the trigonal bipyramidal Sn site in $K_2SnP_2O_7$ is the least negative and at the same time is characterized by the highest η (Table

DOI: 10.1021/acs.jpcb.8b04236
J. Phys. Chem. B 2018, 122, 7416–7425

3). The ^{119}Sn NMR spectra of the SnO−P_2O_5 glasses display the same trend of increasing average δ_{iso} and η with decreasing SnO content (Figure 13). Moreover, the trend of increasing ^{119}Sn δ_{iso} (decreasing shielding) with decreasing SnO content is also consistent with a concomitant increase in the average coordination of Sn, which would result in the lone pair electrons moving away from the nucleus, consequently lowering its shielding.[11] Therefore, it may be argued that a significant fraction of the Sn atoms in these glasses assumes the trigonal bipyramidal environment, and the relative fraction of this environment steadily decreases with increasing Sn content. This hypothesis is consistent with the recent report of the observation by diffraction of Sn atoms being solely in a trigonal pyramidal coordination in a tin phosphate glass of composition 67SnO−33P_2O_5.[30] A progressive change in the conformation of the Sn−O coordination polyhedra is also reflected in the nearly linear increase in $|\delta|$ of the ^{119}Sn chemical shift tensor in these glasses with increasing SnO content (Figure 13). Because increasing $|\delta|$ suggests a decreasing sphericity of the chemical shift tensor, one possible scenario is that the corresponding trend in the conformation of the Sn−O polyhedra involves an increasingly asymmetric disposition of the nearest-neighbor NBOs. Such a conformation is observed in the structure of crystalline β-$Sn_2P_2O_7$, where two of the NBOs bonded to Sn reside on two Q^1 units from the same Q^1 dimer, whereas the other NBO is part of a different Q^1 unit, which results in one O−Sn−O angle substantially larger than the other two, for majority of the Sn sites.[31] However, the validity of such a scenario can only be tested through the systematic future investigation of the effect of conformation of SnO_3 pyramid on its chemical shift tensor, using ab initio calculations. It may be noted here that although the compositional trends of $|\delta|$ and η for ^{119}Sn observed in this study are consistent with those reported in a previous study based on the simulations of static ^{119}Sn NMR line shapes, the trend in ^{119}Sn δ_{iso} was opposite.[11] This discrepancy is possibly the result of the fact that static ^{119}Sn NMR line shapes of glasses are broadened by both large chemical shift dispersion and anisotropy, whose effects could not be separated in the static NMR spectra reported in previous studies.[7,11]

As noted earlier, the SnO−P_2O_5 glasses are characterized by some of the lowest T_g values known for binary phosphate glasses.[33,34] In a previous study, Lim et al. ascribed this behavior to the low coordination number of Sn, which leads to a lower degree of connectivity of the phosphate network.[9] Although this hypothesis is consistent with the predominantly trigonal pyramidal coordination environment of Sn atoms observed in this study, a low coordination number of Sn alone cannot explain the low and nearly composition-independent T_g values. This is because the Sn−O bonds are somewhat stronger than the P−O bonds[9] and the atomic packing increases with increasing Sn content throughout the composition range for glass formation in this system. It is tempting to argue that in addition to its low coordination number, the Sn atoms also display a preference for bonding to two of the three (or, four) NBOs that are on the same Q^2 chain or Q^1 dimer, as observed in the structure of crystalline β-$Sn_2P_2O_7$,[31] which lowers the average network connectivity (Figure 14).

4. CONCLUSIONS

The compositional evolution of the structure of SnO−P_2O_5 glasses is investigated using the high-resolution ^{31}P PASS and ^{119}Sn 2D pjMAT/CPMG NMR spectroscopy. A self-consistent structural model results from the consideration of the full chemical shift tensor for the ^{31}P and the ^{119}Sn nuclides. The Q speciation is found to follow the binary model. With increasing SnO, the phosphate network dominated by the Q^3 and the Q^2 species is gradually replaced by a more closely packed structure consisting of phosphate chains and dimers, i.e., the Q^2 and the Q^1 species. The ^{119}Sn NMR results demonstrate that the Sn atoms are present in both 3-fold and 4-fold coordinations with the NBO atoms in all the glasses, and the relative fraction of the latter decreases with increasing Sn content. The low coordination number of Sn in combination with its preference for bonding to NBOs that are on the same Q^2 chain or Q^1 dimer leads to an unusually low network connectivity that is manifested in rather low and nearly composition-independent T_g values characteristic of the SnO−P_2O_5 glasses.

AUTHOR INFORMATION

Corresponding Author

*E-mail: sbsen@ucdavis.edu.

ORCID

Sabyasachi Sen: 0000-0002-4504-3632

Notes

The authors declare no competing financial interest.

ACKNOWLEDGMENTS

This work was supported by a grant from the National Science Foundation (NSF-DMR 1505185) to S.S. The National High Magnetic Field Laboratory is supported by the National Science Foundation through NSF/DMR-1157490, DMR-1644779, and the State of Florida. The assistance of Nicholas Botto with the use of electron probe microanalysis is very gratefully acknowledged.

REFERENCES

(1) Brow, R. K. Review: The Structure of Simple Phosphate Glasses. *J. Non-Cryst. Solids* **2000**, *263*−*264*, 1−28.

(2) Oelkers, E. H.; Montel, J. Waste Storage. *Elements* **2008**, *4*, 113−116.

(3) Wilder, J. A. Glasses and Glass Ceramics for Sealing to Aluminum Alloys. *J. Non-Cryst. Solids* **1980**, *38*−*39*, 879−884.

(4) Hönninger, C.; Morier-Genoud, F.; Moser, M.; Keller, U.; Brovelli, L. R.; Harder, C. Efficient and Tunable Diode-Pumped Femtosecond Yb:Glass Lasers. *Opt. Lett.* **1998**, *23*, 126.

(5) Martin, V.; Werner-Zwanziger, U.; Zwanziger, J. W.; Dunlap, R. A. Correlation of Structure and Photoelastic Response in Tin Phosphate Glass. *Int. J. Appl. Glass Sci.* **2011**, *2*, 282−289.

(6) Cha, J.; Kubo, T.; Takebe, H.; Kuwabara, M. Compositional Dependence of Properties of SnO − P_2O_5 Glasses. *J. Ceram. Soc. Jpn.* **2008**, *116*, 915−919.

(7) Bekaert, É.; Montagne, L.; Delevoye, L.; Palavit, G.; Revel, B. Structure and Properties of x SnO − (100−x) P_2O_5 Glasses. *C. R. Chim.* **2004**, *7*, 377−382.

(8) Shih, P. Y. Properties and FTIR Spectra of Lead Phosphate Glasses for Nuclear Waste Immobilization. *Mater. Chem. Phys.* **2003**, *80*, 299−304.

(9) Lim, J. W.; Yung, S. W.; Brow, R. K. Properties and Structure of Binary Tin Phosphate Glasses. *J. Non-Cryst. Solids* **2011**, *357*, 2690−2694.

(10) Jäger, C.; Feike, M.; Born, R.; Spiess, H. W. Direct Detection of Connectivities in Glasses by 2D NMR. *J. Non-Cryst. Solids* **1994**, *180*, 91−95.

(11) Holland, D.; Howes, A.; et al. Lone-Pair Effects and Structural Trends in x SnO·(1−x) P_2O_5 Glasses Deduced from ^{31}P and ^{119}Sn

DOI: 10.1021/acs.jpcb.8b04236
J. Phys. Chem. B 2018, 122, 7416−7425

Nuclear Magnetic Resonance. *J. Phys.: Condens. Matter* **2002**, *14*, 13609−13621.
(12) Gan, Z. High-Resolution Chemical Shift and Chemical Shift Anisotropy Correlation in Solids Using Slow Magic Angle Spinning. *J. Am. Chem. Soc.* **1992**, *114*, 8307−8309.
(13) Antzutkin, O. N.; Shekar, S. C.; Levitt, M. H. Two-Dimensional Sideband Separation in Magic-Angle-Spinning NMR. *J. Magn. Reson., Ser. A* **1995**, 7−19.
(14) Levitt, M. H.; Madhu, P. K.; Hughes, C. E. Cogwheel Phase Cycling. *J. Magn. Reson.* **2002**, *155*, 300−306.
(15) Massiot, D.; Fayon, F.; Capron, M.; King, I.; Le Calvé, S.; Alonso, B.; Durand, J. O.; Bujoli, B.; Gan, Z.; Hoatson, G. Modelling One- and Two-Dimensional Solid-State NMR Spectra. *Magn. Reson. Chem.* **2002**, *40*, 70−76.
(16) Hung, I.; Gan, Z. On the Magic-Angle Turning and Phase-Adjusted Spinning Sidebands Experiments. *J. Magn. Reson.* **2010**, *204*, 150−154.
(17) Hung, I.; Edwards, T.; Sen, S.; Gan, Z. MATPASS/CPMG: A Sensitivity Enhanced Magic-Angle Spinning Sideband Separation Experiment for Disordered Solids. *J. Magn. Reson.* **2012**, *221*, 103−109.
(18) Kaseman, D. C.; Hung, I.; Lee, K.; Kovnir, K.; Gan, Z.; Aitken, B.; Sen, S. Tellurium Speciation, Connectivity, and Chemical Order in As_xTe_{100-X} glasses: Results from Two-Dimensional ^{125}Te NMR Spectroscopy. *J. Phys. Chem. B* **2015**, *119*, 2081−2088.
(19) Whittles, Z.; Marple, M.; Hung, I.; Gan, Z.; Sen, S. Structure of BaO-TeO_2 glasses: A Two-Dimensional ^{125}Te NMR Spectroscopic Study. *J. Non-Cryst. Solids* **2018**, *481*, 282−288.
(20) Harris, R. K.; Becker, E. D.; Cabral de Menezes, S. M.; Goodfellow, R.; Granger, P. Commission on Molecular Structure and Spectroscopy. *Pure Appl. Chem.* **2001**, *73*, 1795−1818.
(21) Haeberlen, U. *High Resolution NMR in Solids Selective Averaging: Supplement 1 Advances in Magnetic Resonance*; Elsevier, 2012; Vol. *1*.
(22) Hayashi, A.; Konishi, T.; Tadanaga, K.; Minami, T.; Tatsumisago, M. Preparation and Characterization of SnO-P_2O_5 Glasses as Anode Materials for Lithium Secondary Batteries. *J. Non-Cryst. Solids* **2004**, *345−346*, 478−483.
(23) Kaseman, D. C.; Endo, T.; Sen, S. Structural Disorder and the Effects of Aging in a Phosphate Glass: Results from Two-Dimensional ^{31}P PASS NMR Spectroscopy. *J. Non-Cryst. Solids* **2013**, *359*, 33−39.
(24) Fayon, F.; Massiot, D.; Suzuya, K.; Price, D. L. ^{31}P NMR Study of Magnesium Phosphate Glasses. *J. Non-Cryst. Solids* **2001**, *283*, 88−94.
(25) Glonek, T.; Costello, A. J. R.; Myers, T. C.; Van Warer, J. R. Phosphorus-31 Nuclear Magnetic Resonance Studies on Condensed Phosphates. III . Polyphosphate Spectra. *J. Phys. Chem.* **1975**, *79*, 1214−1218.
(26) Cossement, C.; Darville, J.; Gilles, J.-M.; Nagy, J. B.; Fernandez, C.; Amoureux, J.-P. Chemical Shift Anisotropy and Indirect Coupling in SnO_2 and SnO. *Magn. Reson. Chem.* **1992**, *30*, 263−270.
(27) Mathew, M.; Schroeder, L. W.; Jordan, T. H. The Crystal Structure of Anhydrous Stannous Phosphate, $Sn_3(PO_4)_2$. *Acta Crystallogr., Sect. B: Struct. Sci., Cryst. Eng. Mater.* **1977**, *33*, 1812−1816.
(28) Köhler, J.; Tong, J.; Dinnebier, R.; Simon, A. Crystal Structure and Electronic Structure of Red SnO. *Z. Anorg. Allg. Chem.* **2012**, *638*, 1970−1975.
(29) Weng, S. F.; Chen, K. B.; Lee, C. S. Synthesis and Characterization of Alkali-Metal Tin(II) Phosphates: $Na_{10}Sn_{31}(HPO_4)_6(P_2O_7)_6(PO_4)_{12}$and $K_2SnP_2O_7$. *Solid State Sci.* **2008**, *10*, 1485−1490.
(30) Hoppe, U.; Saitoh, A.; Tricot, G.; Freudenberger, P.; Hannon, A. C.; Takebe, H.; Brow, R. K. The Structure and Properties of xZnO−(67−x)SnO−33P_2O_5 glasses: (II) Diffraction, NMR, and Chromatographic Studies. *J. Non-Cryst. Solids* **2018**, *492*, 68−76.
(31) Chernaya, V. V.; Mitiaev, A. S.; Chizhov, P. S.; Dikarev, E. V.; Shpanchenko, R. V.; Antipov, E. V.; Korolenko, M. V.; Fabritchnyi, P. B. Synthesis and Investigation of Tin (II) Pyrophosphate $Sn_2P_2O_7$. *Chem. Mater.* **2005**, *17*, 284−290.
(32) Bonhomme, C.; Gervais, C.; Babonneau, F.; Coelho, C.; Pourpoint, F.; Azaïs, T.; Ashbrook, S. E.; Griffin, J. M.; Yates, J. R.; Mauri, F.; et al. First-Principles Calculation of NMR Parameters Using the Gauge Including Projector Augmented Wave Method: A Chemists Point of View. *Chem. Rev.* **2012**, *112*, 5733−5779.
(33) Le Saoût, G.; Simon, P.; Fayon, F.; Blin, A.; Vaills, Y. Raman and Infrared Study of $(PbO)_x(P_2O_5)_{(1-x)}$ Glasses. *J. Raman Spectrosc.* **2002**, *33*, 740−746.
(34) Walter, G.; Hoppe, U.; Vogel, J.; Carl, G.; Hartmann, P. The Structure of Zinc Polyphosphate Glass Studied by Diffraction Methods And 31P NMR. *J. Non-Cryst. Solids* **2004**, *333*, 252−262.

DOI: 10.1021/acs.jpcb.8b04236
J. Phys. Chem. B 2018, 122, 7416−7425